Original Research

Serum-derived exosomes from neurofibromatosis type 1 congenital tibial pseudarthrosis impaired bone by promoting osteoclastogenesis and inhibiting osteogenesis

Ge Yang[1,*], Hui Yu[2,*], Yaoxi Liu[1], Weihua Ye[1], Guanghui Zhu[1], An Yan[1], Qian Tan[1] and Haibo Mei[1]

[1]Pediatric orthopedic lab, Department of Orthopedic Surgery, the Hunan Children's Hospital, Hunan 410000, PR China; [2]Department of Orthopedic and Trauma Surgery, University Hospital Bonn, Bonn 39062, Germany

Corresponding authors: Qian Tan. Email: qiantanhnpo@outlook.com; Haibo Mei. Email: meihaiboprof@outlook.com

*These authors contributed equally to this paper.

Impact statement

Congenital pseudarthrosis of the tibia (CPT) is an uncommon and puzzling disease associated with a high rate of disability. To date, the biological mechanisms related to this disease have largely not been elucidated. In this study, we determined the biological functions of serum-derived exosomes (SDEs) from children with neurofibromatosis type 1 (NF1) associated with CPT (CPT-SDEs) and compared their proteomic profiles with those of SDEs from normal children. Based on proteomics analysis, 410 differentially expressed proteins, including 289 downregulated proteins and 121 upregulated proteins, were identified in the CPT-SDEs. In addition, CPT-SDEs decreased the osteogenic differentiation of MC3T3-E1 cells and promoted the osteoclastogenesis ability of RAW264.7 cells. Moreover, injecting CPT-SDEs into the tail veins led to bone loss in rats, as detected by the reduction in trabecular and cortical bone mass. These findings indicate that CPT-SDEs impair bone quality, which may provide a reasonable explanation for the low bone quality and tibial nonunion in children with *NF1* associated with congenital tibial pseudarthrosis.

Abstract

Treatment of congenital pseudarthrosis of the tibia (CPT) still is full of challenges in pediatric orthopedist. Serum-derived exosomes (SDEs) have been proven to be participated in bone remodeling. However, the molecular changes in SDEs of CPT children and their pathologies have not been elucidated. In this study, SDEs were isolated and purified from CPT patients (CPT-SDEs) associated with neurofibromatosis type 1 (NF1) and normal children (Norm-SDEs). Then we obtained the proteomics profile of SDEs by combining liquid chromatography-tandem mass spectrometry (LC-MS/MS) and tandem mass tag label-based quantitation. *In vitro*, the efficacy of SDEs on osteoblastic differentiation of MC3T3-E1 cells and osteoclastogenesis ability of RAW264.7 cells were evaluated by quantitative real-time PCR (qRT-PCR) and cytochemical staining. *In vivo*, we used micro-CT to assess cortical bone mass and trabecular microstructures to reflect the influence of SDEs on bone remodeling after injection into the tail vein of rats. Based on proteomics analysis, 410 differentially expressed proteins, including 289 downregulated proteins and 121 upregulated proteins, were identified in the CPT-SDEs. These proteins have multiple biological functions associated with cellular metabolic processes, catalytic activity, and protein binding, which are important for cell differentiation and proliferation. *In vitro*, CPT-SDEs decreased the osteogenic differentiation of MC3T3-E1 cells and promoted the osteoclastogenesis of RAW264.7 cells. Injection of CPT-SDEs into the tail vein for two months resulted in bone loss in rats, as indicated by the decrease in trabecular and cortical bone mass. Our findings demonstrated the differences in proteins in SDEs between normal and CPT children with NF1. These differentially expressed proteins in CPT-SDEs contributed to deteriorating trabecular bone microstructures by inhibiting bone formation and stimulating bone resorption.

Keywords: Congenital pseudarthrosis of the tibia, exosomes, osteoclast, osteoblast, bone microstructure

***Experimental Biology and Medicine* 2021; 246: 130–141. DOI: 10.1177/1535370220962737**

Introduction

Congenital pseudarthrosis of the tibia (CPT) is a rare and puzzling disease with a variety of clinical manifestations, from tibial anterolateral bowing to spontaneous fractures and nonunion.[1,2] Over the past several decades, various surgeries have regularly been needed by CPT patients to consolidate pseudarthrosis and refracture.[3] However, because the entire tibia cannot raise a normal healing response to fracture injury, treating patients with CPT remains a difficult and challenging task for pediatric orthopedic physicians.

It is well documented that children with CPT are commonly associated with inactivation of the neurofibromatosis type 1 (NF1) gene.[4] Accumulating evidence has demonstrated that the loss of function of the *NF1* gene impairs skeletal development and induces osseous abnormalities.[5] Studies have demonstrated that children with NF1 associated with congenital tibial pseudarthrosis exhibit less osteogenic activity than normal children,[6] and the physiopathologies of these children are related to active osteoclastic resorption and impaired osteoblastic function at the site of the fracture[7,8] or even disrupt systemic skeletal mineral metabolism.[6,9] In addition, biological assays further demonstrate that the ability of mesenchymal stem cells from CPT patients produced a lower proportion of bone-forming cells than in normal individuals,[10,11] and this deficiency was more evident in patients with NF1.[11,12] As cellular metabolism is affected by the surrounding microenvironment, researchers considered that alterations in the microenvironment of patients with NF1 associated with congenital tibial pseudarthrosis might influence bone homeostasis;[13] however, the specific mechanisms governing this effect have largely not been elucidated.

Exosomes are small vesicles measuring 30 to 100 nm in diameter that are secreted by almost all cells and contain various bioactive molecules (proteins, nucleic acids and lipids) to mediate intercellular communication.[14] Normally, exosomes are secreted and transported into the circulatory system to target distant cells to regulate the cellular microenvironment and physiological functions.[14] Recently, serum-derived exosomes (SDEs) have attracted increasing concerns in the field of bone remodeling and have been demonstrated to be involved in some skeletal diseases, such as osteoporosis or osteopenia.[15] Considering that serum contains abundant exosomes, we speculated that SDEs derived from children with NF1 associated with congenital tibial pseudarthrosis (CPT-SDEs) may play a critical role in the pathological process of CPT.

Therefore, to determine the biological functions associated with CPT-SDEs, we compared the proteomic profiles of CPT-SDEs with those of SDEs from normal children (Norm-SDEs). Furthermore, we analyzed the effects of CPT-SDEs on osteogenic and osteoclastic ability *in vivo* and *in vitro*, and we elucidated the hidden mechanisms governing the pathobiology of CPT.

Materials and methods

Study subjects and sample collection

Blood samples were obtained from 12 patients with an atrophic type of CPT (3–8 years old) and from 15 healthy physically examined children (3–6 years old) from June 2017 to August 2019 in the orthopedic department of Hunan Children's Hospital. We combined clinical and radiographic features to diagnose CPT, and all included patients in this study were associated with NF1, which fulfilling the National Institute of Health Consensus Development Conference diagnostic criteria for NF1.[16] None of the children received any treatment before this study, and all information was obtained from Hunan Children's Hospital. With the informed consent of all children's parents, the study was approved by the Ethics Committee of Hunan Children's Hospital.

Exosome isolation

Serum samples were centrifuged to isolate the exosomes, as previously reported.[17] Briefly, whole blood samples were centrifuged at 3500*g* for 30 min to eliminate blood cells or fragments, and serum samples were collected. Then, diluted the serum with an equal volume of phosphate-buffered saline (PBS), filtered it through a 0.22 μm filter, and centrifuge at 25,000*g* at 4°C for 90 min to further remove microparticles remaining in diluted serum after filtration. After that step, the ExoQuick-TC agentia (System Biosciences, Palo Alto, CA, USA) was added to the diluted serum, incubated overnight and recentrifuged to obtain exosomes, and resuspended in 200 μL of PBS. Collected the supernatant (non-exosomal part) of the sample without disturbing the exosomal precipitation. The protein volume of exosomes was assessed by Bradford assay (Bio-Rad Laboratories, Hercules, CA, USA). Finally, all exosomes were stored at −80°C or used for further experiments.

Transmission electron microscopy (TEM)

The morphological evaluation of isolated exosomes was conducted by TEM (Libra120, Carl Zeiss NTS GmbH, Oberkochen, Germany). To this end, the isolated exosomes were placed onto formvar-carbon-coated grids and subsequently stained with 2% ammonium molybdate and observation with an electron microscope at 200 kV. Exosome diameter was measured using ImageJ software, and a histogram was constructed in GraphPad Prism 7.0.

Western blotting analysis

The exosome markers CD63 and ALIX were probed using specific antibodies. For Western blot analysis, the isolated exosomes were washed with PBS and lysed with RIPA buffer. The lysed protein (20 μg total protein) was extracted and separated by 10% SDS-PAGE and then transferred to polyvinylidene fluoride membranes. The membranes were blocked in 5% fat-free milk, and incubated with CD63 (1:200, Abcam, UK) and ALIX (1:10,000, Abcam) primary

antibodies at 4°C overnight. After washing with TBS-0.05% Tween-20 buffer and incubation with the secondary antibodies, the target proteins were imaged with a Fluor Chem E Chemiluminescent Western Blot Imaging System (ProteinSimple, USA). Bradford assay was adopted to as a control to estimate standardized loading.

Labeling was performed using tandem mass tag (TMT)

After trypsin digestion, digested proteins were then desalted, vacuum-dried, and finally dissolved in 200 mmol/L triethylammonium bicarbonate buffer (pH 8.5). TMT kit is used to label the digested proteins according to the manufacturer's protocol. The labeled samples were pooled, desalted, and dissolved in 0.1% trifluoroacetic acid.

High-performance liquid chromatography (HPLC) separation

The TMT-labeled peptides were fractionated by HPLC (UltiMate 3000 UHPLC, Thermo Scientific, MA, USA) equipped with an Xbridge BEH300C18 column maintained at 45°C (5-μm particles, 10-mm ID, 250-mm length). Briefly, the peptides were first separated with a gradient of 8% to 32% acetonitrile (pH 9.0) over 60 min into 60 fractions. Then, the peptides were combined into six fractions and dried by vacuum centrifugation.

Liquid chromatography (LC)-MS/MS analysis

The peptides were dissolved in 0.1% formic acid and separated using an EASY-nLC 1000 ultrahigh-performance liquid chromatography (UPLC) system (Thermo). The gradient was comprised of an increase from 7% to 25% solvent (containing 0.1% formic acid and 90% acetonitrile) for 24 min, 25–40% for 8 min, increasing to 40–80% for 4 min, and then holding at 80% for 4 min at 350 nL/min flow rate. LC-MS/MS analysis was performed according to the protocol from Xu *et al*.[18]

Bioinformatic analysis

The differentially expressed proteins between groups were visualized and identified by a volcano plot using the DAVIDs Functional Annotation Chart tool (Version 6.8) to generate Gene Ontology (GO) annotation and to characterize their biological process, cellular component, and molecular function terms using FunRich software (2.1.2). A protein–protein interaction (PPI) network was constructed using the STRING database (v.10.5), and a novel graph theoretical clustering algorithm, "Molecular Complex Detection" (MCODE), was used to analyze and visualize the densely connected regions in PPI networks using Metascape (http://metascape.org). The most densely connected PPI regions were identified, and the enriched pathways were analyzed using the Kyoto Encyclopedia of Genes and Genomes (KEGG) database ($-\lg(P \text{ value}) > 2$ as threshold). Hierarchical clustering analysis and a heat map were used to construct the extent of differentially expressed proteins among the samples by Cluster3.0 software.

Culture of osteoblast and osteoclast progenitors

RAW264.7 cells were obtained from American Type Culture Collection and cultured in α-minimum essential medium containing penicillin (100 U/mL; Gibco), streptomycin (100 U/m; Gibco), 10% FBS and 10 ng/mL RANKL in 24-well plates. MC3T3-E1 cells (ATCC, Rockville, USA) were induced with differentiation medium supplemented with 50 μg/mL ascorbic acid-2-phosphate and 10 μM β-glycerol phosphate. The cells were incubated at 37°C in 5% CO_2, and the medium was replaced every 2–3 days. SDEs (250 μg) from each group were added to RAW264.7 cells (1.5×10^5 cells/cm^2) and MC3T3-E1 cells (1.5×10^5 cells/cm^2) once and prepared in triplicate.

SDEs uptake assessment

SDEs from each group were labeled with the PKH67 Green Fluorescent Cell Linker Kit (Sigma-Aldrich) according to the manufacturer's protocol. Briefly, SDEs were resuspended in PBS, incubated with 4 μL PKH67 dye and added to 1 mL Diluent C (Sigma-Aldrich) for 5 min at room temperature. PKH67-SDEs were washed with PBS three times to remove free PKH67 dye and transferred into RAW264.7 cells or MC3T3-E1 cells for 5 h at room temperature. Cells were then washed with PBS, fixed with 3% paraformaldehyde, and stained with 0.5 μg/mL DAPI (Abcam). The samples were detected under a confocal fluorescence microscopy.

Quantitative real-time PCR (qRT-PCR) analysis

Total mRNA from samples was extracted using TRIzol reagent (Invitrogen, USA) and purified with RNeasy mini kit (Qiagen, USA) following the manufacturer's protocol. cDNA was synthesized from 1 μg of total RNA using a commercial kit (Fermentas, Burlington, Canada). qRT-PCR was performed using SYBR Green master mix (Thermo Fisher Scientific), and all genes were run in triplicate and normalized to GAPDH. The PCR primers used in this study were as follows:

Tartrate-resistant acid phosphatase (*Trap*): forward, 5′-TGGTCCAGGAGCTTAACTGC-3′ and reverse, 5′-GTCAGGAGTGGGAGCCATATG-3′.

nuclear factor of activated T cells c1 (*Nfatc1*): forward, 5′-CAGTGTGACCGAAGATACCTGG-3′ and reverse, 5′-TCGAGACTTGATAGGGACCCC-3′.

cathepsin K (*Ctsk*): forward, 5′-GCGGCATTACCAA CAT-3′ and reverse, 5′-CTGGAAGCACCAACGA-3′.

BMP-2: forward, 5′-CTGACCACCTGAACTCCAC-3′ and reverse, 5′-CATCTAGGTACAACATGGAG-3′.

Osteocalcin (*OCN*): forward, 5′-CAATAAGGTAGTGAACAGAC-3′ and reverse, 5′-CTTCAAGCCATACTGGTCT-3.

Osterix: forward, 5′-GTCAAGAGTCTTAGCCAAACTC-3′ and reverse, 5′-AAATGATGTGAGGCCAGATGG-3′.

GAPDH: forward, 5′-CACCATGGAGAAGGCCGGGG-3′ and reverse, 5′-GACGGACACATTGGGGGTAG-3′.

Bone resorption, TRAP, and alizarin red staining

For bone resorption assays, osteoclast progenitor RAW264.7 cells were washed with PBS, seeded on an Osteo Assay Surface (Corning, New York, USA) and stimulated with differentiation reagents for five days at room temperature. The areas of multiple pit clusters were photographed and evaluated. For TRAP staining, RAW264.7 cells were fixed with 3.7% formaldehyde, washed with PBS, and analyzed with a TRAP staining kit according to the manufacturer's instructions. Mature osteoclasts were defined as TRAP-positive multinucleated cells and were defined as mature osteoclasts showing more than three nuclei that were identified as osteoclasts and photographed for evaluation of numbers. Matrix mineralization in the osteoblast progenitor MC3T3-E1 cells was determined by Alizarin Red staining (ARS). Twenty-one days after osteogenic induction, cells were fixed with 3.7% formaldehyde, washed with PBS, and then stained with 40 mM Alizarin Red (pH 4.1) according to the manufacturer's instructions.

Animal and SDEs treatments

Male Sprague Dawley (SD) rats (1 month old, weighing 101–132 g) were randomly allocated into three groups, which were administered intravenous injection with Norm-SDEs (150 μg Norm-SDEs in 100 μL PBS, $n = 8$), CPT-SDEs (150 μg CPT-SDEs in 100 μL PBS, $n = 8$) and an equal volume of PBS (100 μL PBS, $n = 8$) via tail vein injection weekly. All rats were housed in wire mesh cages under a controlled light cycle (12 h light and 12 h dark), fed with rat chow *ad libitum* and liberally supplied with water. At eight weeks after the first treatment, the rats were sacrificed, and bone specimens were harvested for further analysis. For SDEs distribution observation, the bone tissues from rats treated with DiR-labeled SDEs or vehicle were fixed with 4% paraformaldehyde for 24 h, decalcified in EDTA (0.5 mol/L) at 4°C for three days, immersed in 30% sucrose aqueous solution for two days at room temperature, and then sectioned into 10-μm-thick slices. DAPI (0.5 μg/mL; Invitrogen) was applied to stain the nuclei and detected under a confocal fluorescence microscopy.

Microcomputed tomography (μCT) analysis

The right tibia was dissected from rats, fixed with 4% paraformaldehyde for 24 h, and used a Skyscan 1176 (Skyscan) to scan at 50 kV and 400 μA with a resolution of 18 μm per pixel. The cross-sectional, sagittal, and coronal images of the proximal tibia were used for three-dimensional histological analysis of bone microstructure. The area of interest selected for analysis began 0.3 mm below the growth plate and extended proximally for 3 mm length to evaluate the trabecular thickness (Tb. Th), trabecular number (Tb. N), and trabecular separation (Tb. Sp). For cortical bone analysis, set the area of interest at the mid-diaphysis of the tibia to evaluate the periosteal perimeter (Ps. Pm), endosteal perimeter (Es. Pm), and cortical thickness (Ct. Th).

Statistical analysis

Statistical analyses were performed using Stata (version 13.0, StataCorp, TX, USA). Two groups were compared using an unpaired *t*-test, and multiple groups were compared by one-way analysis of variance (ANOVA) or Bonferroni posttest. $P < 0.05$ was considered to be significant.

Results

Characterization of SDEs and quantitative expression of SDEs protein profiles

To identify exosomes derived from serum, we assessed exosome markers between exosome pellets and supernatants after centrifugation, and the results showed that exosomes were enriched with the exosome markers CD63 and ALIX but not in the supernatants (Figure 1(a-b)). Moreover, TEM showed that most of these pellets exhibited a typical sphere-shaped morphology, with a diameter ranging from 30 to 100 nm (Figure 1(c) and (d)), to further confirm the identity of exosomes. Next, we used TMT-based proteomics to screen the differentially expressed proteins (1.3-fold change standard and Wilcoxon-test $P < 0.05$ threshold) between CPT-SDEs and Norm-SDEs. In total, 59,997 unique peptides were screened and detected based on the MS/MS spectrum database, corresponding to 1606 proteins, of which 1588 proteins were identified with quantitative overlap of 1350 exosome proteins in the Vesiclepedia database (FunRich software, version 3.1.3; Figure 1(e)). Among these 1588 proteins, 121 proteins were upregulated, and 289 proteins were downregulated, in CPT-SDEs. To further categorize the functions of the 410 differentially expressed proteins, GO annotation was performed and indicated that most of the identified differentially expressed proteins were derived from the chaperone complex and important for the molecular functions of protein folding, nicotinamide adenine dinucleotide, and cofactor binding. These proteins were also involved in the biological processes of nucleoside, ribose, and oxidoreduction coenzyme metabolic processes (Figure 1(f)), which is in keeping with the recorded functions of exosomes.[19] Also, GO annotations for the up- and downregulated proteins are shown in Supplemental Figure S1. Above all, these data indicate that we successfully purified exosomes from serum and that the differentially expressed proteins between CPT-SDEs and Norm-SDEs are mainly involved in the regulation of transcription, metabolism, and cell growth.

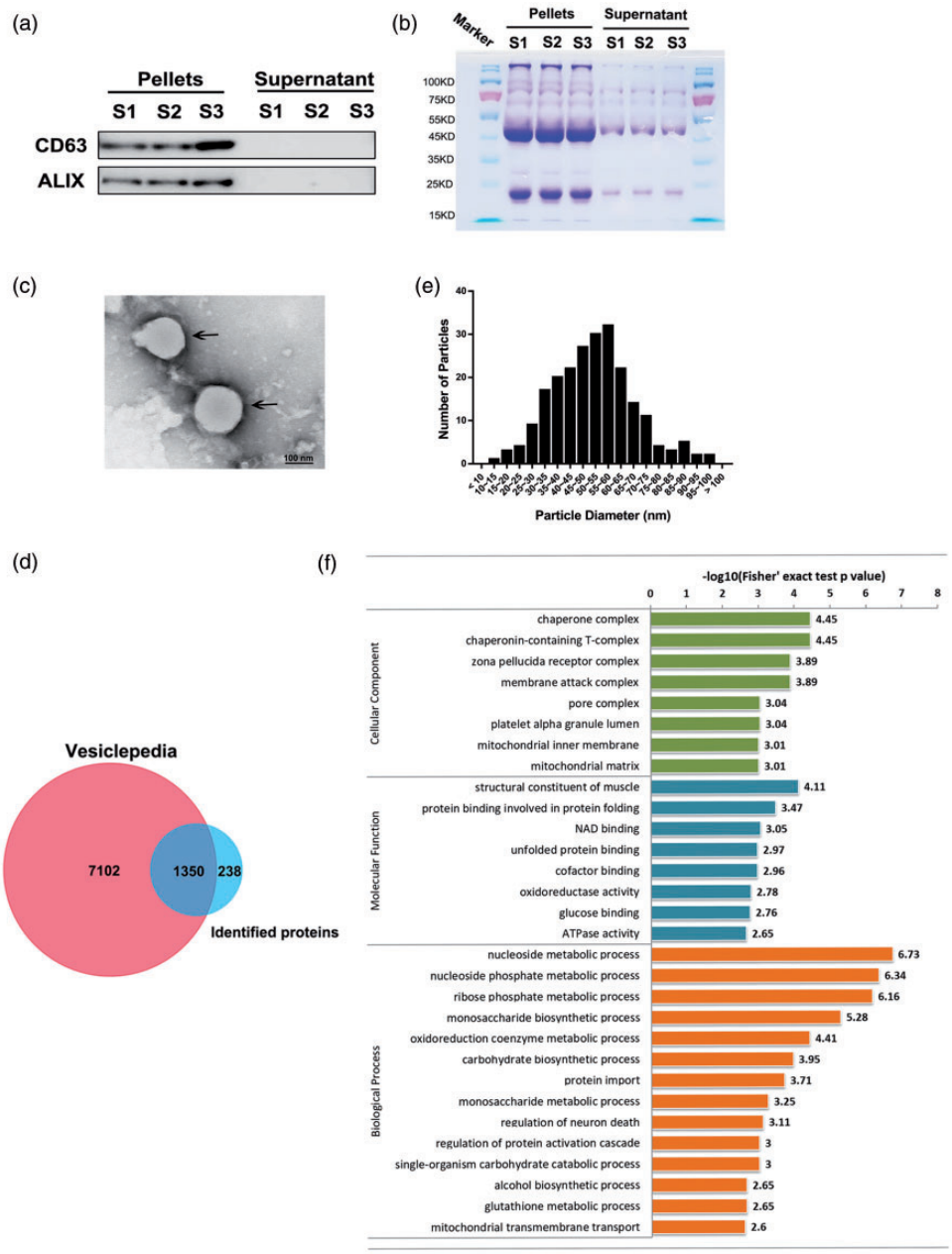

Figure 1. Efficiency of SDEs extraction and proteomics analysis of protein profiles. (a-b) Western blot analysis of exosomal markers in exosome pellets and supernatants. Coomassie Brilliant Blue staining was used as a control to assess standardized loading ($n = 3$ patients per group). (c) Morphology observed by TEM (black arrows). (d) Number of particles with a diameter ranging from 30 to 100 nm. (e) Venn diagram showing the overlap of identified proteins with the FunRich software exome protein database. (f) GO enrichment results showed the top 8 significantly enriched cellular component terms, 8 significantly enriched molecular function terms, and 14 significantly enriched biological process terms (Y-axis: categories of GO terms; X-axis: enrichment score ($-$lg (P value)). (A color version of this figure is available in the online journal.)

Analysis of the important differentially expressed protein component and KEGG enrichment

It has been hypothesized that the identification of the PPI network is crucial to understanding the principles of biological processes and predicting protein functions.[20] Thus, we used MCODE for PPI enrichment analysis to further characterize the differentially expressed proteins between CPT-SDEs and Norm-SDEs. The MCODE analysis revealed that there were 14 MCODE components that the proteins were densely connected (Supplementary Figure S2) and corresponded to their respective biological functions (Supplementary Table S1). Moreover, the most important MCODE component was extracted from the PPI network, which included the 51 most densely connected differentially expressed proteins (Figure 2(a)). Notably, the heatmap showed that all of the most densely connected proteins were significantly downregulated in CPT-SDEs (Figure 2(b)). Next, to further elucidate the biological pathways associated with the most densely connected proteins, we mapped the gene symbol to the KEGG database (Figure 2(c)). The results suggested that a total of 11 pathways were generated from KEGG based on all differentially

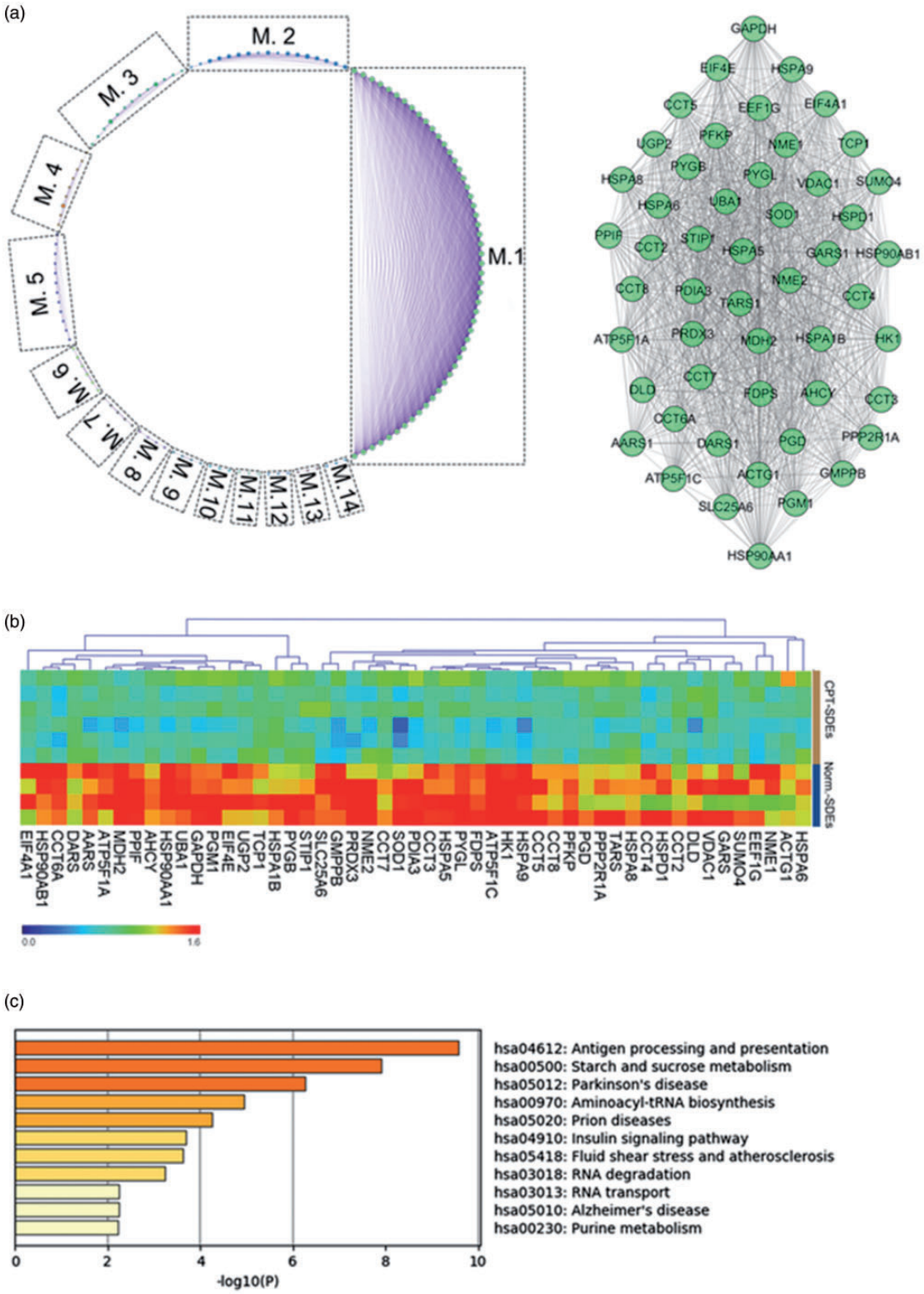

Figure 2. SDEs differentially expressed protein components and KEGG enrichment. (a) The MCODE algorithm showed that M1 was the most densely connected cluster, which contained 51 differentially expressed proteins. (b) Heatmap of differentially expressed proteins between Norm-SDEs and CPT-SDEs (*P* value cut-off: 0.05. fold-value change: ≥1.6). (c) KEGG analysis of the biological pathways associated with the most densely connected proteins. (A color version of this figure is available in the online journal.)

expressed proteins. These 51 differentially expressed proteins were enriched in hsa04612 antigen processing and presentation ($-\lg p = -9.582$) followed by hsa000500 energy metabolism ($-\lg p = -7.910$), hsa05012 Parkinson's disease ($-\lg p = -6.269$), and some other pathways. The related proteins of hsa04612 antigen processing and presentation included HSP90AA1, HSP90AB1, PDIA3 and some other proteins. HK1, PGM1, PYGB, and some other proteins

were involved in hsa000500 energy metabolism. In addition, SLC25A6, ATP5F1A, ATP5F1C, UBA1, VDAC1, PPIF, and SOD1 were associated with hsa05012 Parkinson's disease (Supplementary Table S2).

CPT-SDEs inhibit osteogenesis in vitro

To observe the effect of CPT-SDEs in osteoblasts, CPT-SDEs were added to treat MC3T3-E1 cells. Our results showed that SDEs labeled with PKH67 dye (green fluorescence) were successfully taken up by MC3T3-E1 cells (Figure 3 (a)). Then, qRT-PCR analysis was performed to determine osteogenic activities, which showed that the transcription of osteogenesis-related genes, such as *BMP-2*, *OCN*, and *Osterix*, were significantly decreased in CPT-SDE-treated cells compared with the Norm-SDE-treated cells and the control group (Figure 3(b)). ARS was also performed to determine the matrix mineralization in the MC3T3-E1 cells after 21 days of induction, which showed that CPT-SDEs significantly reduced matrix mineralization compared with the control and Norm-SDE-treated cells (Figure 3(c)). Additionally, the osteogenic activities reflected by the degree of matrix mineralization of Norm-SDE-treated cells were significantly upregulated compared with control cells, which indicated that Norm-SDEs possessed osteogenic potential. Taken together, our data indicated that Norm-SDEs promoted osteogenic ability, while CPT-SDEs had a precise effect in reducing osteogenesis.

CPT-SDEs promote osteoclastogenesis in vitro

To assess the effects of CPT-SDEs on osteoclasts *in vitro*, RAW264.7 cells were cultured with SDEs treatment, and PKH67 labeling confirmed that the SDEs were successfully taken up by RAW264.7 cells (Figure 4(a)). We then performed qRT-PCR analysis to determine osteoclastic activities, which showed that the transcription of osteoclastogenesis-related genes, such as *Ctsk*, *Nfatc1*, and *Trap*, were significantly upregulated in CPT-SDE-treated cells compared with the control and Norm-SDE-treated cells (Figure 4(b)). TRAP staining further showed that the numbers of osteoclasts were markedly increased after CPT-SDEs treatment compared with the control cells and Norm-SDE-treated cells (Figure 4(c)). Additionally, a significant reduction in both osteoclastic activities and

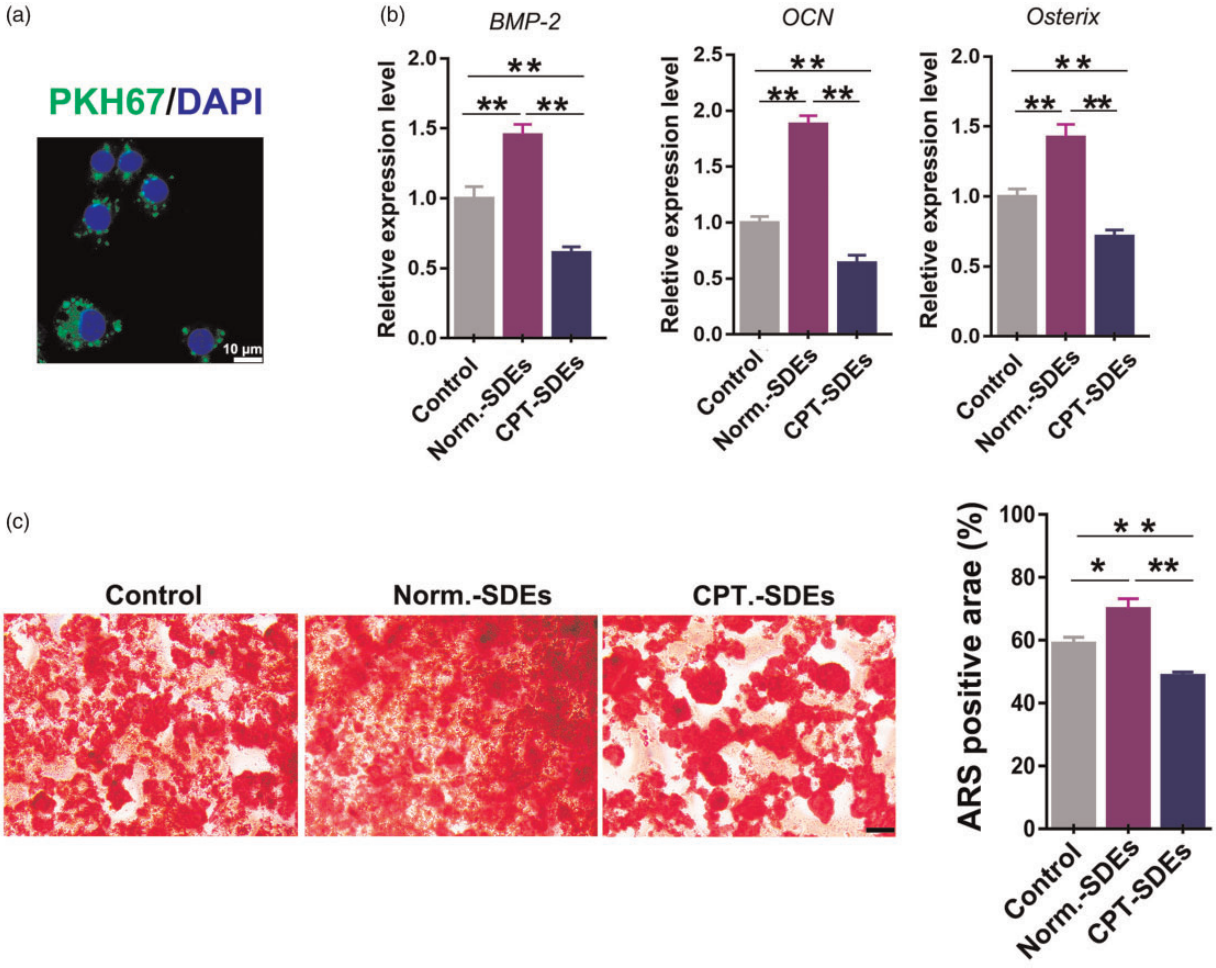

Figure 3. CPT-SDEs inhibit MC3T3-E1 cell osteogenesis activities. (a) Fluorescence images showing PKH67-labeled CPT-SDEs (green) uptake by MC3T3-E1 cells. Scale bar: 10 μm. (b) qRT-PCR analyses were performed to evaluate the transcription levels of *BMP-2*, *OCN*, and *Osterix* in the control, Norm-SDE-, and CPT-SDE-treated cells. (c) Quantification of ARS staining and the relative mineralization level. Scale bar: 100 μm. $^{*}P < 0.05$, $^{**}P < 0.01$. (A color version of this figure is available in the online journal.)

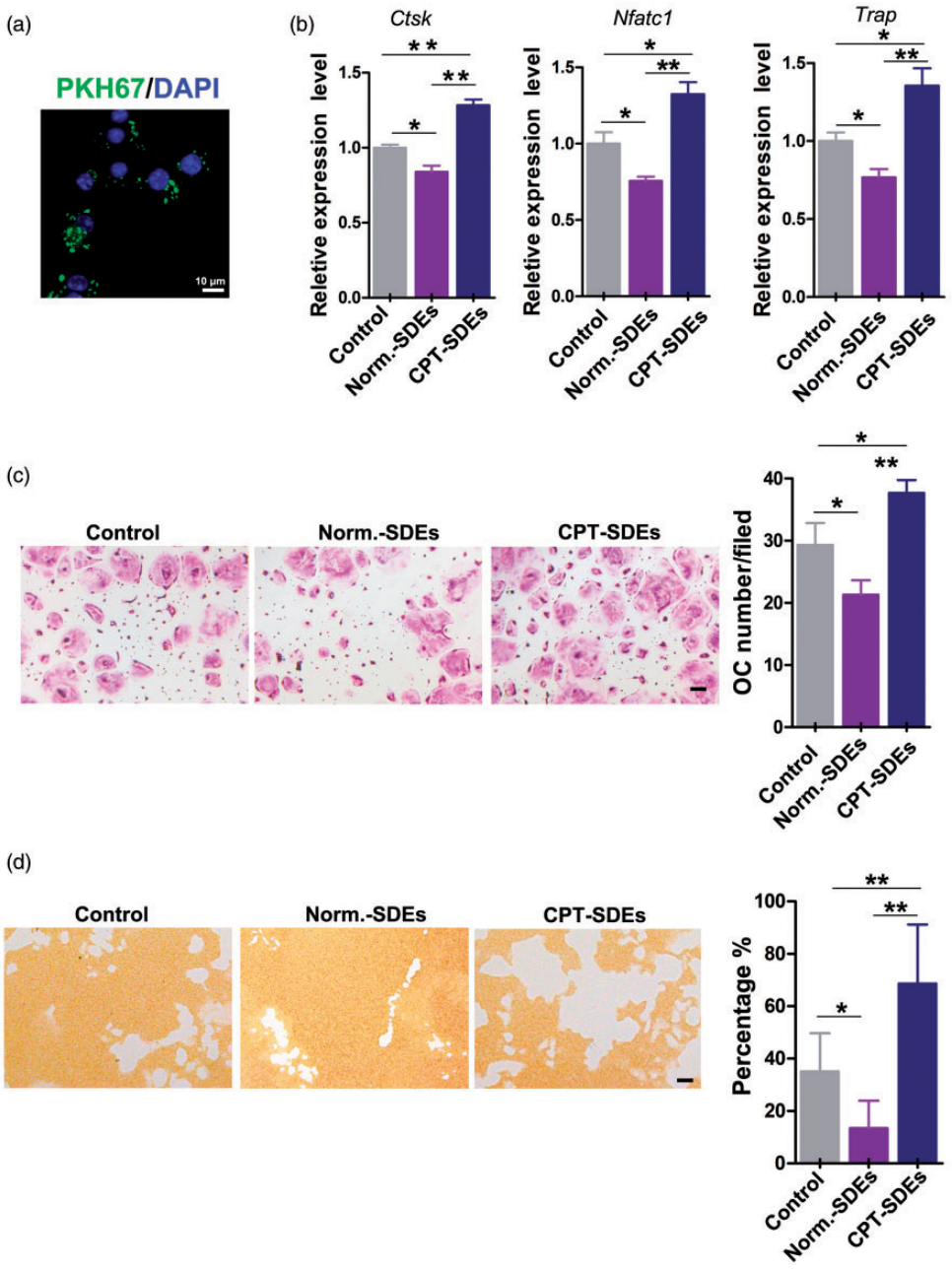

Figure 4. CPT-SDEs promote RAW264.7 cell osteoclastogenesis activities. (a) Fluorescence images showing PKH67-labeled SDEs (green) uptake by RAW264.7 cells. Scale bar: 10 μm. (b) qRT-PCR analysis was performed to evaluate the transcription levels of *Ctsk*, *Nfatc1*, and *Trap* in the control, Norm-SDE- and CPT-SDE-treated cells. (c) Quantification of TRAP staining and the numbers of TRAP-positive osteoclasts per field of view. Scale bar: 100 μm. (d) Representative images show the bone resorption of RAW264.7 cells cultured with CPT-SDEs or Norm-SDEs. Scale bar: 10 μm. $^{*}P < 0.05$, $^{**}P < 0.01$. (A color version of this figure is available in the online journal.)

proliferation was also observed after Norm-SDEs treatment compared with control cells. Consistent with the observed osteoclast proliferation, the bone resorption of RAW264.7 cells cultured with CPT-SDEs was significantly stronger than the resorption of osteoclasts cultured with Norm-SDEs. Interestingly, we found that Norm-SDEs had a slightly inhibited effect on RAW267.4 resorption ability compared with the control (Figure 4(d)). Taken together, our data indicated that CPT-SDEs could promote osteoclast differentiation *in vitro*.

CPT-SDEs aggravate bone loss in vivo

To determine whether CPT-SDEs exerted a bone-loss effect *in vivo*, one-month-old rats were treated with CPT-SDEs, Norm-SDEs, and an equal volume of PBS by intravenous injection. In bone tissues, SDEs predominantly accumulated on trabecular bone surfaces, where active bone formation or bone remodeling often occurs (Figure 5(a)). μCT scanning was performed to show that tibial trabeculae and cortical bone mass were lower after CPT-SDEs

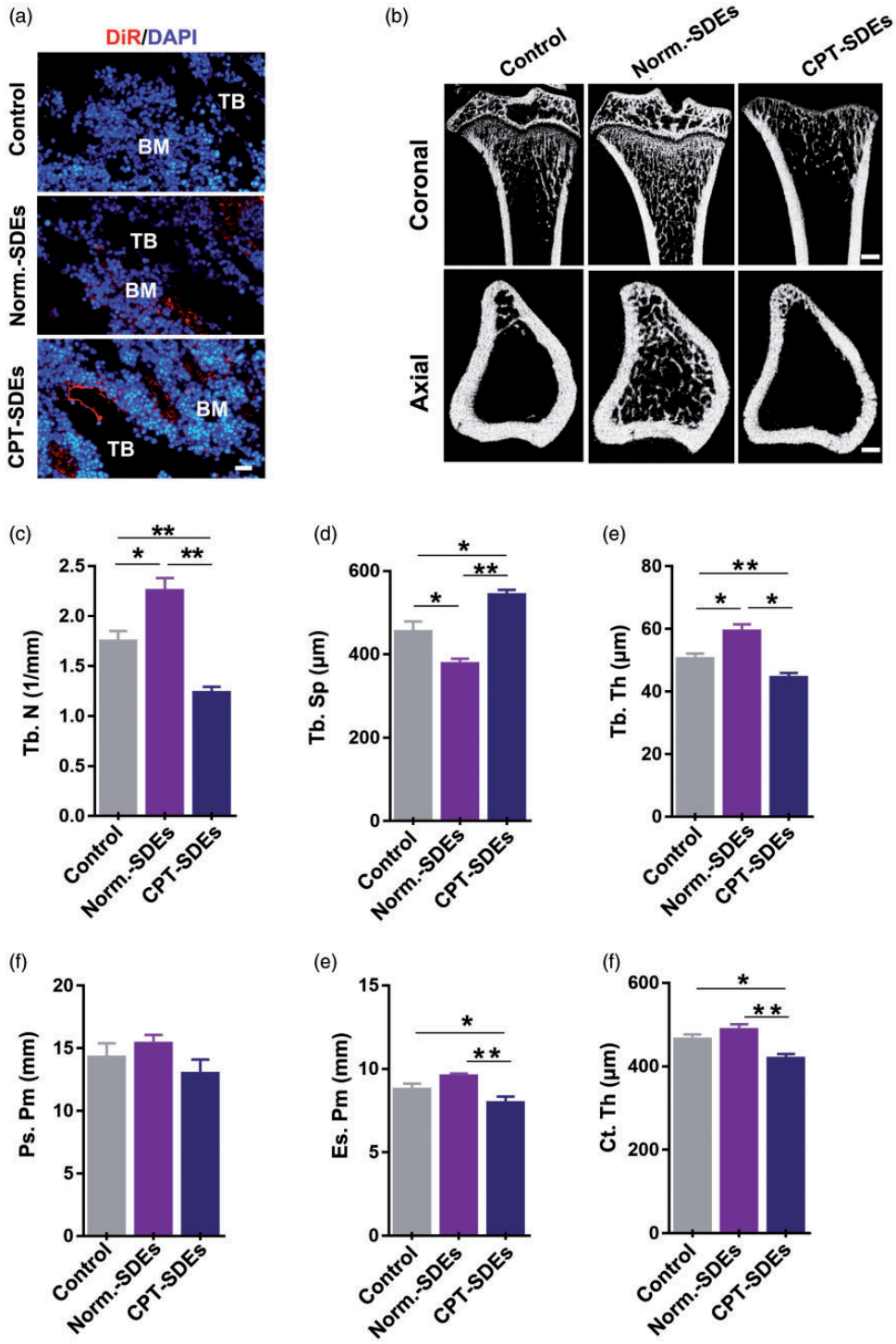

Figure 5. CPT-SDEs impaired bone microstructure quality in young rats. (a) Fluorescence images show tibial tissue sections from vehicle-treated rats and rats intravenously injected with DiR-labeled SDEs for 3 h. TB: trabecular bone; BM: bone marrow. Scale bar: 20 μm. (b) Representative μCT images of the tibia. Scale bars: 1 mm. (c to f) Quantitative μCT analysis of the trabecular number (Tb. N), trabecular separation (Tb. Sp), trabecular thickness (Tb. Th), periosteal perimeter (Ps. Pm), endosteal perimeter (Es. Pm), and cortical thickness (Ct. Th). $n = 5$ per group. $^{*}P < 0.05$, $^{**}P < 0.01$. (A color version of this figure is available in the online journal.)

treatment compared with control and Norm-SDE-treated rats after eight weeks of administration (Figure 5(b)). Quantitative analysis further confirmed that trabecular thickness and number decreased and that trabecular separation increased with CPT-SDEs treatment compared to control and Norm-SDE-treated rats (Figure 5(c) to (e)). Consistent with the observations made in trabecular bone, the cortical bone thickness and endosteal perimeter significantly decreased with CPT-SDE treatment compared to control and Norm-SDE-treated rats (Figure 5(f) and (g)). Taken together, our data indicated that CPT-SDEs treatment could impair bone microstructure quality in rats.

Discussion

It has been widely considered that fibrous hamartoma at the pseudarthrosis site is the main pathology of CPT.[3] Although resection of fibrous hamartoma tissue is a key step in treatment protocols, it cannot insure union or prevent latter refracture.[3] In the present study, we analyzed the differential expression of proteins in SDEs by TMT-based high-throughput proteomics strategy, and we detected some crucial differential proteins that may be involved in some crucial biological processes and functions in bone homeostasis and remodeling. Moreover, intravenous injection of CPT-SDEs impaired bone microstructure in rats, as verified by decreased tibial trabeculae and cortical bone mass, by inhibiting osteogenic activities and promoting osteoclast differentiation. These findings demonstrated that CPT-SDEs may be associated with systemic bone metabolic disease.

Exosomes are diminutive natural membrane vesicles that contain a specific set of proteins and serve as mediators of intercellular communication in the microenvironment.[14] Using TMT-based high-throughput proteomic tactic to detect the differential proteins in SDEs helped to elucidate the pathogenesis of CPT. In this study, with a 1.3-fold change cutoff, we discovered that 121 proteins in the CPT-SDEs were increased compared with the normal children, while 289 were decreased. To provide insight into the biological functions related to all the differentially expressed proteins in CPT-SDEs, GO analysis was performed and revealed that the upregulated proteins were predominantly enriched in the biological process of transport and immune response while being downregulated in metabolism, energy pathway, and cell growth factors. Using MCODE analysis, we found that these differentially expressed proteins can be divided into 14 components and identified that the most densely connected component (containing 51 proteins) was related to protein folding and regulation of protein localization. As densely connected proteins do not take effect without connections but have complex interactions, we used KEGG analysis to analyze these proteins and revealed that they were mainly involved in the biological processes of metabolism and energy pathways. Consequently, these differential proteins and the network components support the idea that CPT-SDEs may play a crucial role in the pathogenesis of NF1 congenital tibial pseudarthrosis.

Our results found that the 51 differentially expressed proteins in the most densely connected network component were all downregulated in CPT-SDEs. Using GO annotation, we found that these downregulated proteins were primarily involved in ATP metabolism (e.g. ATP5F1A, ATP5F1C, and CCT2), heat shock proteins (e.g. HSPA8, HSPA9, and HSP90AA1), carbohydrate metabolism (e.g. HK1, GMPPB, and GAPDH), and glycine metabolism (e.g. DLD, GARS, and PDIA3). Hoebertz *et al.* demonstrated that ATP at low concentrations strongly inhibited bone formation.[21] In addition, previous studies have suggested that changes in HSP,[22,23] carbohydrate metabolism[24] or glycine metabolism-related protein families[25] also disrupt the balance of bone homeostasis. Thus, these densely connected proteins may state novel ideas for thorough research and help to identify new therapeutic agents for NF1 associated with CPT.

Based on the bioinformatic results, we further explored the effects of the differentially expressed proteins in SDEs on the formation of osteoblast and osteoclast. In our study, we elucidated that CPT-SDEs could be taken up by cells and notably improved osteoclastic differentiation of RAW264.7 cells, as detected by the increased TRAP-positive cells and bone resorption, as well as increased expression levels of osteoclastogenesis-related genes. On the other hand, the CPT-SDEs could also suppress osteogenesis, as proven by reduced matrix mineralization and down-expressed levels of osteogenesis-related genes. Hence, the adverse impact of CPT-SDEs on bone remodeling may be attributed to its function in the role of regulating endogenous osteoblasts and osteoclasts.

SDEs have been identified as major contributing factors in regulating the bone microenvironment and pathogenesis.[26,27] To verify whether the CPT-SDEs can cause abnormal bone metabolism, we detected the bone microstructure after intravenous injection of SDEs in rats. In accordance with the *in vitro* studies, intravenous injection of CPT-SDEs effectively impaired bone microstructures in rats, which was defined as decreased trabecular and cortical bone mass, attenuated osteogenic activities and enhanced osteoclast formation. SDEs in the circulatory system are crucial paracrine mediators that affect the bone metastatic microenvironment and remodeling.[15,26] Notably, our results illustrated that the transcription of osteoclastogenesis-related genes was downregulated, while the transcription of osteogenesis-related genes was upregulated, in Norm-SDEs compared with the control. These data demonstrated that Norm-SDEs have a significantly protective effect on bone metabolism. Previous studies also showed that the osteogenic potential of mesenchymal stem cells was lower when cultured in serum from patients with NF1 associated with congenital tibial pseudarthrosis, suggesting that the released factors of the circulatory system could be a key question in CPT.[12,13] Taken together, our study proved that SDEs can regulate rat bone microstructure and reflect an exact molecular explanation for the low bone mass and quality of CPT patients.

Using bioinformatic analysis, for the first time, we collected SDEs from NF1 congenital tibial pseudarthrosis and normal children and identified the differentially expressed proteins, revealing the potential biological processes between them. In addition to revealing the potential biological process of differentially expressed proteins, the effects of CPT-SDEs on osteoblastic and osteoclastic differentiation and function were assessed. Moreover, in accordance with the inhibition of osteoblastic activity and enhancement of osteoclastic activity *in vitro*, the rats exhibited an impaired bone microstructure quality after treatment with CPT-SDEs compared with the Norm-SDEs. As this study was a pilot observational study, the molecular mechanism underlying SDEs and bone remodeling was not studied. Although a correlation between CPT-SDEs and impaired bone microstructure quality was observed, the

role and mechanism of CPT-SDEs remain to be further investigated.

In general, our results demonstrate that CPT-SDEs reduce bone mass and quality in rats. The mechanism governing this reduction may be the regulation of the functional characteristics of osteoblasts and osteoclasts, as CPT-SDEs can inhibit osteogenic activity and promote osteoclastic differentiation and function *in vitro*. Furthermore, bioinformatic analysis revealed that bone remodeling changes may be ascribed to differentially expressed proteins and altered biological processes. Our data suggest that CPT-SDEs are important microenvironmental factors associated with the pathological mechanisms of NF1 associated with congenital tibial pseudarthrosis.

Authors' contributions: GY, HY, QT, and HM conceived and designed the study. GY, HY, and YL performed the experimental analysis, GY and HY wrote the manuscript. GZ, AY, and WY collected the serum samples. The authors read and approved the final manuscript.

ACKNOWLEDGMENTS

The authors thank Ms Wanli Dong and Weiran Ye for their generous assistance during the preparation of the manuscript.

DECLARATION OF CONFLICTING INTERESTS

The author(s) declare no potential conflicts of interest with respect to the research, authorship, and/or publication of this article.

FUNDING

The author(s) disclosed receipt of the following financial support for the research, authorship, and/or publication of this article: This study was supported by the Natural Science Foundation of Hunan Province (No. 2020JJ5282), the Futang Children's Science Foundation of China (No. FTCSF-2018-02), the Clinical Research Center for Limb Deformity of Children in Hunan Province (2019SK4006), the China Postdoctoral Science Foundation (No. 2019M652773), the 2019 Annual Scientific Research Project of Hunan Provincial Health and Family Planning Commission Science Foundation (No. 20190664), and the 2020 Annual Scientific Research Project of Hunan Provincial Health and Family Planning Commission Science Foundation (No. 20200390).

ETHICAL APPROVAL

The experimental protocol was approved by the Research Ethics Committee of Hunan Children's Hospital. Informed consent was obtained from every patient.

ORCID iD

Haibo Mei https://orcid.org/0000-0002-9434-1716

SUPPLEMENTAL MATERIAL

Supplemental material for this article is available online.

REFERENCES

1. Hardinge K. Congenital anterior bowing of the tibia. The significance of the different types in relation to pseudarthrosis. *Ann R Coll Surg Engl* 1972;**51**:17–30
2. Hefti F, Bollini G, Dungl P, Fixsen J, Grill F, Ippolito E, Romanus B, Tudisco C, Wientroub S. Congenital pseudarthrosis of the tibia: history, etiology, classification, and epidemiologic data. *J Pediatr Orthop B* 2000;**9**:11–5
3. Paley D. Congenital pseudarthrosis of the tibia: biological and biomechanical considerations to achieve union and prevent refracture. *J Child Orthop* 2019;**13**:120–33
4. Van Royen K, Brems H, Legius E, Lammens J, Laumen A. Prevalence of neurofibromatosis type 1 in congenital pseudarthrosis of the tibia. *Eur J Pediatr* 2016;**175**:1193–8
5. Lee DY, Cho TJ, Lee HR, Lee K, Moon HJ, Park MS, Yoo WJ, Chung CY, Choi IH. Disturbed osteoblastic differentiation of fibrous hamartoma cell from congenital pseudarthrosis of the tibia associated with neurofibromatosis type I. *Clin Orthop Surg* 2011;**3**:230–7
6. Leskela HV, Kuorilehto T, Risteli J, Koivunen J, Nissinen M, Peltonen S, Kinnunen P, Messiaen L, Lehenkari P, Peltonen J. Congenital pseudarthrosis of neurofibromatosis type 1: impaired osteoblast differentiation and function and altered NF1 gene expression. *Bone* 2009;**44**:243–50
7. Cho TJ, Seo JB, Lee HR, Yoo WJ, Chung CY, Choi IH. Biologic characteristics of fibrous hamartoma from congenital pseudarthrosis of the tibia associated with neurofibromatosis type 1. *J Bone Joint Surg Am* 2008;**90**:2735–44
8. Ippolito E, Corsi A, Grill F, Wientroub S, Bianco P. Pathology of bone lesions associated with congenital pseudarthrosis of the leg. *J Pediatr Orthop B* 2000;**9**:3–10
9. Petramala L, Giustini S, Zinnamosca L, Marinelli C, Colangelo L, Cilenti G, Formicuccia MC, D'Erasmo E, Calvieri S, Letizia C. Bone mineral metabolism in patients with neurofibromatosis type 1 (von Recklingausen disease). *Arch Dermatol Res* 2012;**304**:325–31
10. Granchi D, Corrias MV, Garaventa A, Baglio SR, Cangemi G, Carlini B, Paolucci P, Giunti A, Baldini N. Neuroblastoma and bone metastases: clinical significance and prognostic value of Dickkopf 1 plasma levels. *Bone* 2011;**48**:152–9
11. Granchi D, Devescovi V, Baglio SR, Magnani M, Donzelli O, Baldini N. A regenerative approach for bone repair in congenital pseudarthrosis of the tibia associated or not associated with type 1 neurofibromatosis: correlation between laboratory findings and clinical outcome. *Cytotherapy* 2012;**14**:306–14
12. Granchi D, Devescovi V and Baglìo SR. Biological basis for the use of autologous bone marrow stromal cells in the treatment of congenital pseudarthrosis of the tibia. *Bone* 2010;**46**:780–8
13. Diaz-Solano D, Wittig O, Mota JD, Cardier JE. Isolation and characterization of multipotential mesenchymal stromal cells from congenital pseudoarthrosis of the tibia: case report. *Anat Rec* 2015;**298**:1804–14
14. Meldolesi J. Exosomes and ectosomes in intercellular communication. *Curr Biol* 2018;**28**:R435–R44
15. Xie Y, Gao Y, Zhang L, Chen Y, Ge W, Tang P. Involvement of serum-derived exosomes of elderly patients with bone loss in failure of bone remodeling via alteration of exosomal bone-related proteins. *Aging Cell* 2018;**17**:e12758
16. Gutmann DH, Aylsworth A, Carey JC, Korf B, Marks J, Pyeritz RE, Rubenstein A, Viskochil D. The diagnostic evaluation and multidisciplinary management of neurofibromatosis 1 and neurofibromatosis 2. *JAMA* 1997;**278**:51–7
17. Chen Y, Xie Y, Xu L, Zhan S, Xiao Y, Gao Y, Wu B, Ge W. Protein content and functional characteristics of serum-purified exosomes from patients with colorectal cancer revealed by quantitative proteomics. *Int J Cancer* 2017;**140**:900–13
18. Xu J, Lan H, Fang H, Huang X, Zhang H, Huang J. Quantitative proteomic analysis of the rice (Oryza sativa L.) salt response. *PLoS One* 2015;**10**:e0120978
19. Kowal J, Arras G, Colombo M, Jouve M, Morath JP, Primdal-Bengtson B, Dingli F, Loew D, Tkach M, Thery C. Proteomic comparison defines

novel markers to characterize heterogeneous populations of extracellular vesicle subtypes. *Proc Natl Acad Sci U S A* 2016;**113**:E968–77
20. Li M, Wu X, Wang J, Pan Y. Towards the identification of protein complexes and functional modules by integrating PPI network and gene expression data. *BMC Bioinformatics* 2012;**13**:109
21. Hoebertz A, Mahendran S, Burnstock G, Arnett TR. ATP and UTP at low concentrations strongly inhibit bone formation by osteoblasts: a novel role for the P2Y2 receptor in bone remodeling. *J Cell Biochem* 2002;**86**:413–9
22. Fujita K, Otsuka T, Kawabata T, Sakai G, Matsushima-Nishiwaki R, Kozawa O, Tokuda H. Inhibitors of heat shock protein 90 augment endothelin1induced heat shock protein 27 through the SAPK/JNK signaling pathway in osteoblasts. *Mol Med Rep* 2018;**17**:8542–7
23. Kai H, Chenyi Y, Erman C, Wei Z, Deting X. Role of the heat shock protein family in bone metabolism. *Cell Stress Chaperones* 2018;**23**:1153–64
24. Karner CM, Long F. Glucose metabolism in bone. *Bone* 2018;**115**:2–7
25. Qi X, Liu Y, Ding ZY, Cao JQ, Huang JH, Zhang JY, Jia WT, Wang J, Liu CS, Li XL. Synergistic effects of dimethyloxallyl glycine and recombinant human bone morphogenetic protein-2 on repair of critical-sized bone defects in rats. *Sci Rep* 2017;**7**:42820
26. Behera J, Tyagi N. Exosomes: mediators of bone diseases, protection, and therapeutics potential. *Oncoscience* 2018;**5**:181–95
27. Wang X, Guo B, Li Q, Peng J, Yang Z, Wang A, Li D, Hou Z, Lv K, Kan G, Cao H, Wu H, Song J, Pan X, Sun Q, Ling S, Li Y, Zhu M, Zhang P, Peng S, Xie X, Tang T, Hong A, Bian Z, Bai Y, Lu A, Li Y, He F, Zhang G, Li Y. miR-214 targets ATF4 to inhibit bone formation. *Nat Med* 2013;**19**:93–100

(Received May 11, 2020, Accepted September 9, 2020)